Acta Biochim Biophys Sin (2009): 603–617 | © The Author 2009. Published by ABBS Editorial Office in association with Oxford University Press on behalf of the Institute of Biochemistry and Cell Biology, Shanghai Institutes for Biological Sciences, Chinese Academy of Sciences. DOI: 10.1093/abbs/gmp048.
Advance Access Publication 8 June 2009

# Functional and structural alterations induced by copper in xanthine oxidase

Mahnaz Hadizadeh[1], Ezzatollah Keyhani[2], Jacqueline Keyhani[2]*, and Cyrus Khodadadi[1]

[1]Institute of Biochemistry and Biophysics, University of Tehran, PO Box 13145-1384, 13145 Tehran, Iran
[2]Laboratory of Life Sciences, Saadat Abade, Sarve Sharghi 58, 19979 Tehran, Iran
*Correspondence address. Tel: +98-21-66956974; E-mail: keyhanie@ibb.ut.ac.ir or keyhanius2002@yahoo.com

**Xanthine oxidase (XO), a key enzyme in purine metabolism, produces reactive oxygen species causing vascular injuries and chronic heart failure. Here, copper's ability to alter XO activity and structure was investigated *in vitro* after pre-incubation of the enzyme with increasing $Cu^{2+}$ concentrations for various periods of time. The enzymatic activity was measured by following XO-catalyzed xanthine oxidation to uric acid under steady-state kinetics conditions. Structural alterations were assessed by electronic absorption, fluorescence, and circular dichroism spectroscopy. Results showed that $Cu^{2+}$ either stimulated or inhibited XO activity, depending on metal concentration and pre-incubation length, the latter also determining the inhibition type. $Cu^{2+}$–XO complex formation was characterized by modifications in XO electronic absorption bands, intrinsic fluorescence, and α-helical and β-sheet content. Apparent dissociation constant values implied high- and low-affinity $Cu^{2+}$ binding sites in the vicinity of the enzyme's reactive centers. Data indicated that $Cu^{2+}$ binding to high-affinity sites caused alterations around XO molybdenum and flavin adenine dinucleotide centers, changes in secondary structure, and moderate activity inhibition; binding to low affinity sites caused alterations around all XO reactive centers including FeS, changes in tertiary structure as reflected by alterations in spectral properties, and drastic activity inhibition. Stimulation was attributed to transient stabilization of XO optimal conformation. Results also emphasized the potential role of copper in the regulation of XO activity stemming from its binding properties.**

*Keywords* xanthine oxidase; enzyme activity; spectroscopy; metal–enzyme complex; copper

Received: January 23, 2009 Accepted: April 3, 2009

## Introduction

Copper is a vital micronutrient involved in a wealth of biological processes [1,2]. Besides its key role in aerobic life as the essential redox-active center in cytochrome c oxidase and its role in the protection against free radical damage as a cofactor for superoxide dismutase, copper is also the active center in a variety of metalloproteins such as dopamine β-hydroxylase, tyrosinase, lysyl oxidase, and ascorbic oxidase [2–4]. In addition, copper participates in various processes including the insertion of molybdenum into molybdopterin [5]. But in spite of its indispensability for cell survival, copper is toxic at elevated levels and a number of disorders have been associated with excess copper [6,7] as well as with copper deficiency [1]. Although a number of specific intracellular copper-binding proteins have been identified, nonspecific binding of the metal to proteins also occurs that will inevitably lead to structural and functional alterations of those proteins with variable consequences for cellular activities and survival [2]. It is thus important to investigate the effect of copper on the structure and activity of individual enzymes. Of particular interest are enzymes, like xanthine oxidase (XO) (EC 1.2.3.2), that carry out essential functions but are also involved in a variety of pathologies caused by the by-products of the enzymatic reaction. Because of its wide distribution in cells and its binding properties, copper could play a regulatory role in these enzymes activity and help in the prevention of their damaging effects.

XO, a complex molybdoflavo protein, is a key enzyme in purine metabolism that has been isolated from a wide range of organisms, including bacteria and men [8,9]. It has attracted lots of attention because of its potential role in tissue and vascular injuries, as well as in inflammatory diseases and chronic heart failure [10,11]. It catalyzes the oxidation of hypoxanthine to xanthine and that of xanthine

to uric acid with concomitant reduction of molecular oxygen [8]. This last step results in the production of superoxide anion and hydrogen peroxide, two reactive oxygen species that have been associated with the potential damaging role of the enzyme [8,11,12]. XO has long been known to be present in bovine milk which remains a main source for purified preparations of the enzyme. Extensive studies conducted with bovine milk XO have led to its characterization and to a proposed mechanism of action. The enzyme is a 290-kDa homodimer, each monomer acting independently in catalysis [13]. The monomer is composed an N-terminal 20-kDa domain containing two iron–sulfur centers (Fe/S I and Fe/S II), a central 40-kDa flavin adenine dinucleotide (FAD) domain, and a C-terminal 85-kDa molybdopterin-binding domain with the four redox centers aligned in an almost linear fashion [13–15]. Substrate oxidation occurs at the molybdenum site, which becomes reduced from $Mo^{VI}$ to $Mo^{IV}$ in the process [16]. The catalytic cycle is completed by electron transfer from molybdenum to the [$Fe_2$–$S_2$] clusters and then to the flavin, where the electrons are donated to an acceptor such as $O_2$ [13,14]. The UV/visible electronic absorption spectrum of the enzyme includes contributions from each reactive center with the iron–sulfur centers exhibiting maxima at 420, 470, and 550 nm, the flavin exhibiting a maximum at 450 nm, and the molybdenum co-factor exhibiting absorption at 350 nm [14,17–19].

The production of reactive oxygen species by XO and its damaging consequences has prompted investigations into the ability of some compounds, such as allopurinol, nitric oxide, or macrocyclic copper II, to control and/or inhibit the enzyme activity, or scavenge the free radicals produced [10,20,21]. Alterations of XO activity by various metals have also been probed with mixed results of either stimulation or inhibition, depending on the metal [22–25]. As mentioned above, because of its ubiquity and its ability to bind to proteins, copper would be one of the metals to probe in priority. However, although partial inhibition of XO activity by $Cu^{2+}$ has been reported [22], there is no thorough investigation on the effect of the metal on the enzyme activity and structure, nor on the potential attachment sites for the metal.

In this study, stimulation as well as inhibition of XO activity by $Cu^{2+}$ is reported along with a detailed investigation on structural changes caused by the metal. Enzymatic activity alterations were assessed by steady-state kinetics studies of the XO-catalyzed oxidation of xanthine to uric acid in the presence of various $Cu^{2+}$ concentrations. Conformational changes around each reactive center were assessed by monitoring changes to the respective electron absorption bands as well as to the visible portion of the circular dichroism (CD) spectrum of the enzyme. Overall structural alterations were studied by fluorescence spectroscopy and far-UV CD spectroscopy. On the basis of the results, a scheme for the sequential attachment of several $Cu^{2+}$ ions per monomer is proposed in relation with the activity alterations observed. Preliminary results of this work were presented as an abstract [26].

## Materials and Methods

### Materials

Xanthine oxidase (bovine milk XO) and xanthine were obtained from Sigma Chemical Co. (St Louis, MO, USA). $CuSO_4$ and all the other chemicals used in this study were obtained from Merck Chemical Co. (Darmstadt, Germany) and were of reagent grade. All buffers and solutions were prepared in water that had been filtered, passed through a mixed bed ion-exchange column, and then distilled. Divalent cations contamination in the chemicals used did not exceed 10 p.p.m. and was at least 10 times diluted in the solutions.

### Enzyme assay

XO activity was measured spectrophotometrically by following the oxidation of xanthine to uric acid at 295 nm, using an extinction coefficient of 9.6 $mM^{-1}\,cm^{-1}$. The assay was performed in 0.1 M citrate-phosphate-borate buffer (hereafter designated assay buffer), pH 7.5, since a preliminary pH profile indicated 7.5 as the optimum pH. Xanthine stock solutions (0.13 mM) were prepared by dissolving xanthine in 1 mM NaOH. XO stock solutions for activity assay were prepared daily by diluting the enzyme in 0.1 M assay buffer, pH 7.5. Enzyme concentrations were determined spectrophotometrically using an extinction coefficient of 36 $mM^{-1}\,cm^{-1}$ at 450 nm. For kinetics studies, the final enzyme concentration in the assay was 6 nM, unless otherwise specified. The reaction was started by the addition of xanthine (final concentration 4–11 μM); the final volume of the reaction mixture was always 3 ml. The enzyme showed an $A_{280}/A_{450}$ value of 5.6; the calculated AFR (activity to flavin ratio) value for the enzyme was 140–150 that corresponds to 65–75% functional enzyme [27].

For assays done in the presence of $Cu^{2+}$ ions, appropriate amounts of $CuSO_4$ stock solution (1.5 M, prepared in distilled water) were added to XO in 0.1 M assay buffer, pH 7.5, and the mixture was incubated at room temperature (22–25°C) for either 0, 5, 10, 20, or 30 min.

Care was taken to maintain the pH at 7.5. The concentration of $Cu^{2+}$ varied from 0.5 μM to 2 mM and XO concentration was 6 nM. The assay was then started by adding xanthine as described above.

Recovery studies were conducted by pre-incubating the enzyme and the metal as described above at room temperature for either 0 or 30 min and then dialyzing the mixture at 4°C against 1 l of assay buffer for 10, 30, and 60 min, with one change of buffer after 30 min. Activity assays were conducted as described above immediately after dialysis.

All results were the average of at least three separate experiments.

### Spectroscopic studies

Electronic absorption spectra were recorded from 250 to 700 nm on a Cary 100 Bio UV−VIS spectrophotometer. For any given spectrum, XO (2.2 μM) and $Cu^{2+}$ (at the desired concentration) in 0.1 M assay buffer, pH 7.5, were added to the sample cuvette and the buffer and $Cu^{2+}$ (at the same concentration as in the sample cuvette) were added to the reference cuvette. For each assay, the enzyme was pre-incubated 5 min (or any other period of time as specified) with 50 μM to 2 mM $Cu^{2+}$, then the absorption spectrum was immediately recorded.

Intrinsic fluorescence was detected on a Cary Eclipse Fluorescence spectrophotometer equipped with temperature controller. Excitation wavelengths of 280 and 295 nm, specific, respectively, for both tryptophan and tyrosine residues and for tryptophan residues alone, were chosen. Emission spectra were recorded between 310 and 500 nm after pre-incubation of 0.28 μM XO with various $Cu^{2+}$ concentrations (5 μM to 2 mM) for increasing periods of time (0−30 min).

CD spectra were recorded with an Aviv Model 215 CD spectrometer. Measurements were done using a 1-mm light path cell for far-UV studies and a 1-cm light path cell for visible studies. The enzyme concentration was 0.86 μM for far-UV studies and 4.7 μM for studies in the visible range. $Cu^{2+}$ concentrations varied from 0.001 to 2 mM.

All spectroscopic measurements were performed at 25°C.

## Results

### Steady-state kinetics studies of XO activity in the presence of $Cu^{2+}$

XO activity was assayed by following the rate of oxidation of xanthine to uric acid. The effect of $Cu^{2+}$ on the XO-catalyzed oxidation of xanthine was investigated by following, at 295 nm and under steady-state conditions, the rate of formation of uric acid after pre-incubation of XO with increasing $Cu^{2+}$ concentrations for various periods of time. The pH activity profile of the enzyme exhibited a peak at 7.5 [**Fig. 1(A),** inset] that was but slightly shifted to pH 7.3 in the presence of $Cu^{2+}$ [**Fig. 1(A)**]; thus all assays were performed at pH 7.5. Pre-incubation of XO (6 nM) with $Cu^{2+}$ (0.5 μM to 2 mM) led to either an increase or a decrease in enzymatic activity depending on both $Cu^{2+}$ concentration and the length of the pre-incubation period [**Fig. 1(B)**]. Addition of less than 5 μM $Cu^{2+}$ to XO resulted either in a stimulation of the enzymatic activity, observable immediately after $Cu^{2+}$ addition (0-min pre-incubation) and after 5- and 10-min pre-incubation [**Fig. 1(B),** closed symbols, $-6.3 \leq \log \leq -5.3$], or in an inhibition of the activity, observable after 20- and 30-min pre-incubation [**Fig. 1(B),** open symbols, $-6.3 \leq \log \leq -5.3$]. Addition of higher $Cu^{2+}$ concentrations resulted in inhibition of the activity, regardless of the pre-incubation length; the inhibition was moderate for $Cu^{2+}$ of 5−700 μM [**Fig. 1(B),** closed and open symbols, $-5.3 \leq \log \leq -3.2$] and drastic when $Cu^{2+}$ concentrations went from 700 to 2000 μM [**Fig. 1(B),** closed and open symbols, $-3.2 \leq \log \leq -2.7$] with no activity detectable in the presence of 2000 μM $Cu^{2+}$ (log = −2.7). Kinetics assays performed with lower (3 nM) or higher (8 nM) enzyme concentrations showed a 5% decrease in stimulation at lower enzyme concentrations and a 4% increase at higher enzyme concentrations, whereas the inhibition increased for lower enzyme concentrations and decreased for higher enzyme concentrations.

The type of inhibition depended solely on the length of the pre-incubation period. Inverse plots obtained after 5-min pre-incubation of XO (6 nm) and $Cu^{2+}$ at different metal concentrations are shown in **Fig. 1(C).** The plots were linear with a common intercept on the abscissa, indicating non-competitive inhibition at $Cu^{2+}$ concentrations of 5 μM and above. Similar plots were obtained when XO activity was assayed immediately after $Cu^{2+}$ addition (0-min pre-incubation) or after 10-min pre-incubation of the enzyme with the metal. For all three pre-incubation times (0-, 5-, or 10-min), the apparent $K_m$ value, which was equal to 9.6 ± 0.1 μM for the control, remained unaffected. The value of the enzyme's apparent $V_{max}$, on the other hand, decreased steadily as the metal concentration increased from 5 to 1500 μM; for a given $Cu^{2+}$ concentration, the decrease in apparent $V_{max}$ intensified as the pre-incubation time went from 0 to 10 min

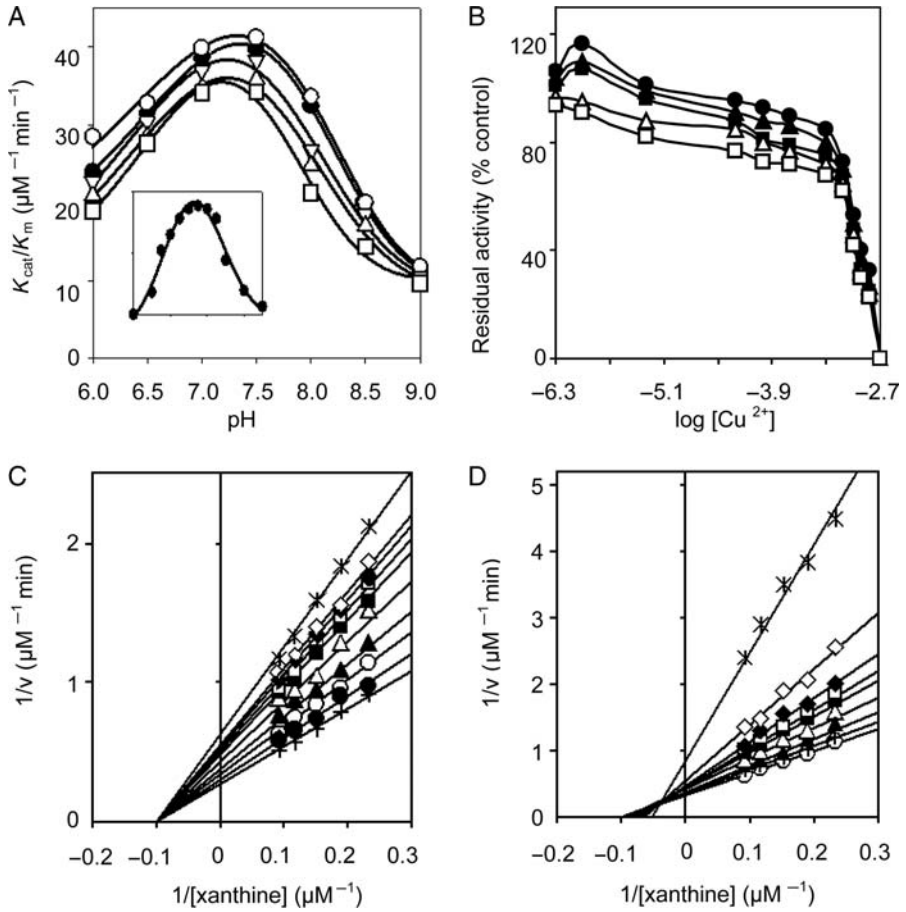


**Figure 1 Steady-state kinetics studies of XO activity in the presence of $Cu^{2+}$** (A) XO pH activity profile in the presence of increasing $Cu^{2+}$ concentrations. XO (8 nM) was pre-incubated with $Cu^{2+}$ (0.001, 0.1, 0.5, and 1 mM) in 0.1 M citrate-phosphate-borate buffer at various pHs (6.0–9.0), for 5 min at room temperature (~22–25°C) before assaying for enzymatic activity. (filled circle) Control; (open circle) 0.001 mM $Cu^{2+}$; (inverted triangle) 0.1 mM $Cu^{2+}$; (triangle) 0.5 mM $Cu^{2+}$; (open square) 1 mM $Cu^{2+}$. Inset: control XO activity profile from pH 4–11. (B) Residual enzymatic activity at optimal pH: XO (6 nM) was pre-incubated with $Cu^{2+}$ (0.0005, 0.001, 0.005, 0.05, 0.1, 0.2, 0.5, 0.75, 1, 1.2, 1.5, and 2 mM) in 0.1 M buffer, pH 7.5, respectively, for 0 min. (filled circle), 5 min (filled triangle), 10 min (filled square), 20 min (triangle), and 30 min (open square) before assaying for enzymatic activity. The copper concentrations were expressed as log of the molar concentrations. Results were the average of at least three separate experiments. (C and D) Inverse plots of 1/rate vs. 1/[xanthine] obtained after 10 min (C) and 20 min (D) pre-incubation of XO with $Cu^{2+}$. Aliquots of the pre-incubated enzyme and metal were placed in a 1-ml reaction mixture of 0.1 M buffer, pH 7.5 and 4–11 μM xanthine; the final enzyme concentration was 6 nM. The rate of uric acid formation was calculated using $\epsilon_{295} = 9.6\ mM^{-1}\ cm^{-1}$. Copper concentrations were 0 (open circle), 0.5 (filled circle), 1 (+), 5 (filled triangle), 50 (triangle), 300 (filled square), 500 (open square), 700 (filled diamond), 900 (diamond), and 1500 (asterisk) μM.

(e.g. from 8 to 15% decrease for 5 μM $Cu^{2+}$ or from 47 to 61% decrease for 1500 μM $Cu^{2+}$). Inverse plots obtained after 20-min pre-incubation of XO and $Cu^{2+}$ at different metal concentrations are shown in **Fig. 1(D).** The plots exhibited a common intercept that was no longer on the abscissa, but above it and to the left of the ordinate, indicating mixed inhibition of XO activity by $Cu^{2+}$. Similar plots were obtained after 30-min pre-incubation of the enzyme with increasing metal concentrations. The values obtained for the enzyme apparent $V_{max}$ and $K_m$ after 20- and 30-min pre-incubation with $Cu^{2+}$ are listed in **Table 1**. For both pre-incubation times, the value of $V_{max}$ decreased while that of $K_m$ increased with increasing metal concentration; the effect of the metal was exacerbated with prolonged pre-incubation.

$K_i$ values were obtained as the intercepts on the abscissa from replots of the slopes ($K_{m,app}/V_{max,app}$) vs. [$Cu^{2+}$]. $K_i$ decreased by approximately a factor of 3 as pre-incubation between XO and $Cu^{2+}$ was prolonged to 30 min. It went from $1.50 \pm 0.05$ to $1.15 \pm 0.05$, $0.90 \pm 0.05$, $0.68 \pm 0.05$, and $0.60 \pm 0.05$ mM as the

**Table 1 Values for XO $V_{max}$ and $K_m$ obtained after 20-or 30-min pre-incubation of the enzyme with various $Cu^{2+}$ concentrations**

| | 20-min pre-incubation | | 30-min pre-incubation | |
|---|---|---|---|---|
| $[Cu^{2+}]$ (μM) | $V_{max}$ (μM $min^{-1}$) | $K_m$ (μM) | $V_{max}$ (μM $min^{-1}$) | $K_m$ (μM) |
| 0 | 2.94 ± 0.2 | 9.6 ± 0.1 | 2.94 ± 0.2 | 9.6 ± 0.1 |
| 0.5 | 2.78 ± 0.06 | 10.0 ± 0.2 | 2.70 ± 0.04 | 10.9 ± 0.07 |
| 1 | 2.70 ± 0.09 | 10.3 ± 0.1 | 2.60 ± 0.03 | 10.6 ± 0.05 |
| 5 | 2.63 ± 0.1 | 10.9 ± 0.1 | 2.56 ± 0.05 | 11.2 ± 0.05 |
| 50 | 2.40 ± 0.06 | 12.2 ± 0.1 | 2.35 ± 0.05 | 12.5 ± 0.08 |
| 300 | 2.25 ± 0.06 | 12.8 ± 0.05 | 2.27 ± 0.08 | 13.5 ± 0.06 |
| 500 | 2.17 ± 0.1 | 13.3 ± 0.05 | 2.15 ± 0.1 | 13.7 ± 0.06 |
| 700 | 2.06 ± 0.04 | 14.1 ± 0.06 | 1.96 ± 0.05 | 14.9 ± 0.05 |
| 900 | 1.85 ± 0.05 | 15.5 ± 0.08 | 1.75 ± 0.05 | 15.8 ± 0.08 |
| 1500 | 1.16 ± 0.05 | 19.2 ± 0.1 | 1.10 ± 0.04 | 20.0 ± 0.1 |
| 2000 | Not detectable | | Not detectable | |

Xanthine was the reducing substrate.

pre-incubation time went from 0 to 5, 10, 20 and 30 min, respectively, an indication of the stabilization of the metal–enzyme complex as the pre-incubation time increased.

### Effect of $Cu^{2+}$ on the catalytic efficiency of the enzyme

$Cu^{2+}$-induced variations in XO catalytic efficiency are illustrated in **Fig. 2**. For up to 10-min pre-incubation (closed symbols), the value of $K_{cat}/K_m$ was larger than the control value when $Cu^{2+}$ concentrations did not exceed 5 μM. The increase peaked for 1 μM $Cu^{2+}$ and was time-dependent, being maximum (27 ± 3%) after 0-min pre-incubation, and diminishing by half (12 ± 2%) after 10-min pre-incubation. When $Cu^{2+}$ concentrations increased from 5 to 700 μM ($-5.3 \leq \log \leq -3.2$), a progressive decrease in catalytic efficiency was observed that became more abrupt when $Cu^{2+}$ concentrations increased from 700 to 1500 μM ($-3.2 \leq \log \leq -2.8$). Pre-incubation of the enzyme with the metal for 20 and 30 min (open symbols) led to a steady decrease in catalytic efficiency as $Cu^{2+}$ concentrations went from 0.5 to 700 μM ($-6.3 \leq \log \leq -3.2$) and to a sharp decrease in catalytic efficiency when $Cu^{2+}$ concentration increased from 700 to 1500 μM ($-3.2 \leq \log \leq -2.8$), with a slope steeper than that observed for 0-, 5-, and 10-min pre-incubation. No activity was detectable in the presence of 2000 μM $Cu^{2+}$, regardless of the pre-incubation time. These results showed that the decrease in XO catalytic efficiency was moderate over a wide range of $Cu^{2+}$ concentrations, but it became much more drastic once a critical metal concentration (0.7 mM) was reached.

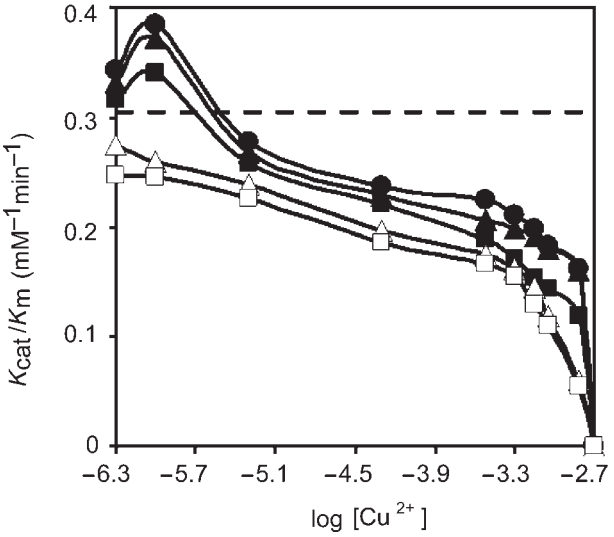


**Figure 2 XO catalytic efficiency as a function of the log of $Cu^{2+}$concentrations (expressed in mol/l)** The ratio $K_{cat}/K_m$ was calculated for XO pre-incubated 0 min (filled circle), 5 min (filled triangle), 10 min (filled square), 20 min (triangle), or 30 min (open square) with 0.5–2000 μM $Cu^{2+}$. Results were the average of at least three separate experiments. The dotted line represents the control value for the enzyme in the absence of $Cu^{2+}$.

The $Cu^{2+}$-induced changes in XO catalytic efficiency were monitored at different pH values (pH 6–9), and no pH-related effect was observed within that range except for a slight shift in the optimum from 7.5 to 7.3 but without alterations in either the acidic or the basic limb.

**Figure 1(A)** illustrates the results obtained after 0-min pre-incubation; similar plots were obtained after 30-min pre-incubation.

Dialysis of the enzyme pre-incubated with various metal concentrations resulted in at least partial restoration of the enzymatic activity. Up to 70% of the enzymatic activity was recovered for $Cu^{2+}$ concentrations without exceeding 0.7 mM, and ~60% of the enzymatic activity was recovered for higher $Cu^{2+}$ concentrations.

## Binding of $Cu^{2+}$ to XO

*Optical characterization of XO–$Cu^{2+}$ complex* The electronic absorption spectrum of native XO shown in **Fig. 3(A)** exhibited essentially four maxima, respectively, at 277, 350, 450, and 550 nm, characteristic of the enzyme [14,17–19]. The highest peak, at 277 nm, was due to the aromatic amino acid side chains, the shoulder at 350 nm was attributed to the molybdenum cofactor [18], the peak at 450 nm and the shoulder at 550 nm were due, respectively, to the FAD and Fe/S centers [14,17]. Two shoulders, due to the Fe/S centers and flanking the 450-nm peak, were detectable at 420 and 470 nm, respectively. Absorption spectra obtained after 5 min incubation of XO with 0.05–2 mM $Cu^{2+}$ are shown in **Fig. 3(B).** The absorption spectra were modified so that decreases in the absorption bands at 350, 450, and 550 nm were observed, indicating alterations around each reactive center in the enzyme. The extent of these spectral alterations was metal concentration-dependent. Concomitantly the absorbance at 277 nm decreased progressively as $Cu^{2+}$ concentration increased and was, in addition, red-shifted for $Cu^{2+}$ concentrations of 0.7 mM and above. The red-shift was progressive and went from 6 nm at 0.7 mM $Cu^{2+}$ to as much as 28 nm at 2 mM $Cu^{2+}$. Spectra obtained after longer pre-incubations were similar to those shown in **Fig. 3(B)** except for accrued decreases in the absorption bands.

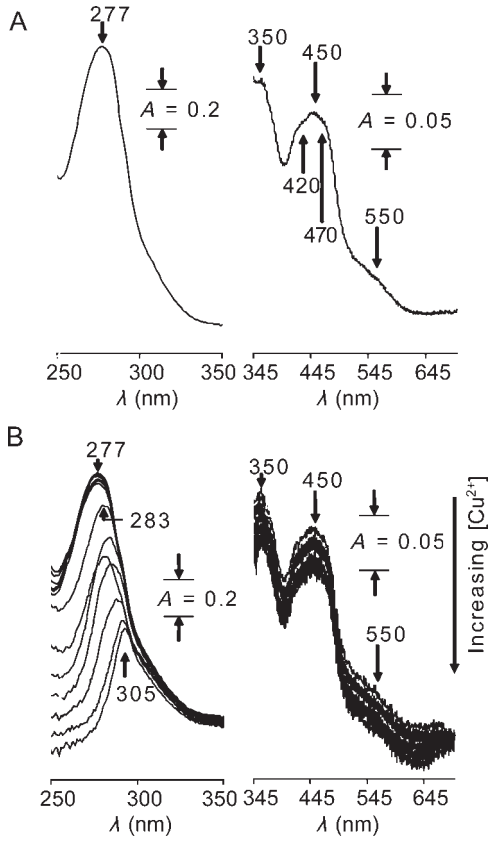


**Figure 3 Electronic absorption spectra of XO (A) and XO incubated with $Cu^{2+}$ (B)** For any given spectrum, XO (2.2 μM), buffer (0.1 M, pH 7.5), and $Cu^{2+}$ (50 μM to 2 mM) were added to the sample cuvette, whereas buffer (0.1 M, pH 7.5) and $Cu^{2+}$ (at the same concentration as in the sample cuvette) were added to the reference cuvette. Spectra were recorded after 5-min pre-incubation of XO with $Cu^{2+}$.

The apparent dissociation constant, $K_d$, of the XO–$Cu^{2+}$ complex was calculated according to Equation (1).

$$1/\Delta A = K_d/\Delta A_{max}\,1/[Cu^{2+}] + 1/\Delta A_{max} \qquad (1)$$

where $\Delta A$ is the absorbance change at a specific wavelength caused by a given $Cu^{2+}$ concentration, $\Delta A_{max}$ is the absorbance change at the specific wavelength for the complete formation of the complex (at infinite $Cu^{2+}$ concentration), and $[Cu^{2+}]$ is the concentration of free $Cu^{2+}$, which is assumed equal to the initial $Cu^{2+}$ concentration [28,29].

In parallel with the alterations in enzymatic activity that were time- as well as $Cu^{2+}$ concentration-dependent, the apparent dissociation constants thus calculated decreased with increasing pre-incubation time. As an illustration, plots of $1/\Delta A_{450}$ vs. $1/[Cu^{2+}]$ corresponding to 5-, 10-, 20-, and 30-min pre-incubation of the enzyme with the metal are shown in **Fig. 4**. Data were gathered from spectral measurements obtained for the full range of $Cu^{2+}$ concentrations investigated (0.05–2 mM). All the plots in **Fig. 4** exhibited two slopes, one corresponding to $Cu^{2+}$ concentrations ranging from 0.05 to 0.7 mM and the other corresponding to $Cu^{2+}$ concentrations ranging from 0.7 to 2 mM. Accordingly, two $K_d$ values, $K_{d1}$ and $K_{d2}$, were calculated; the value of each $K_d$ decreased with increasing pre-incubation time, with $K_{d1}$ exhibiting a more drastic decrease (from $104 \pm 15$ mM after 5-min pre-incubation to $30 \pm 5$ mM after 30-min pre-incubation) than $K_{d2}$ (from $442 \pm 50$ mM after

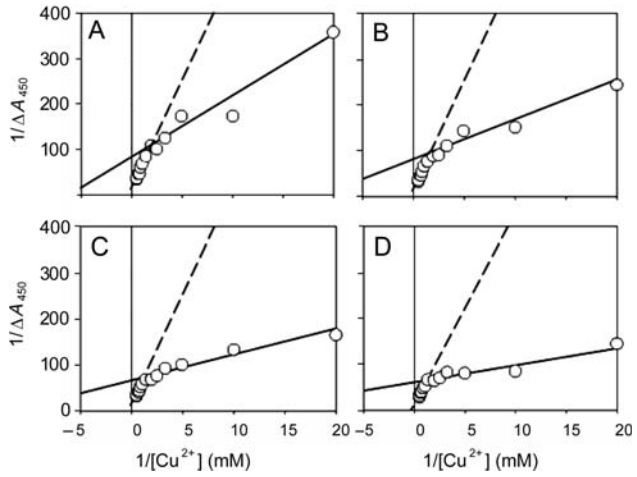


**Figure 4 Inverse plots, $1/\Delta A_{450}$ vs. $1/[Cu^{2+}]$, giving apparent dissociation constants $K_{d1}$ (filled line) and $K_{d2}$ (dotted line), after pre-incubation of XO with $Cu^{2+}$ for different time** $K_{d1}$ was found for $[Cu^{2+}]$ 0.05–0.7 mM (points on the graphs correspond to 0.05, 0.1, 0.2, 0.3, 0.4, 0.5, 0.7 mM $Cu^{2+}$) and $K_{d2}$ was found for $[Cu^{2+}]$ 0.7–2 mM (points on the graph correspond to 0.7, 0.9, 1.1, 1.3, 1.5, 1.75, 2 mM $Cu^{2+}$). The slopes decreased as the pre-incubation time increased and correspondingly the value of $K_{d1}$ and of $K_{d2}$ was, respectively, 104 and 442 mM after 5-min pre-incubation (A), 65 and 387 mM after 10-min pre-incubation (B), 40 and 324 mM after 20-min pre-incubation (C), 30 and 315 mM after 30-min pre-incubation (D).

5-min pre-incubation to 315 ± 30 mM after 30-min pre-incubation) [**Fig. 4(A–D)**].

Two $K_d$ values were also found when the absorbance changes at 350 nm were monitored, but the values were twice as high as those obtained for the absorbance at 450 nm ($K_{d1}$ of 247 ± 25 mM and $K_{d2}$ of 807 ± 90 mM after 5-min pre-incubation of XO with $Cu^{2+}$). A single value for $K_d$ (359 ± 10 mM after 5-min pre-incubation) was found with the absorbance changes recorded at 550 nm. In all cases, $K_d$ values decreased with increasing pre-incubation time (**Figs. 5** and **6**, insets). These results suggested the existence of at least two attachment sites that exhibited different affinities for $Cu^{2+}$ and that would differentially affect the various reacting centers of the enzyme.

Correlatively, two $K_d$ values ($K_{d1}$ of 30 ± 3 mM and $K_{d2}$ of 1.7 ± 0.1 mM after 5-min pre-incubation of XO with $Cu^{2+}$) were found when the absorbance changes at 277 nm were monitored although here $K_{d1}$ was larger than $K_{d2}$; whereas $K_{d1}$ value decreased with increasing pre-incubation time, $K_{d2}$ value remained fairly constant (**Fig. 7**, insets). In parallel with the steady-state kinetics findings that 0.7 mM $Cu^{2+}$ marked the onset for drastic inhibition of the enzymatic activity, and the same critical metal concentration marked the change in apparent dissociation constant for the metal–enzyme complex.

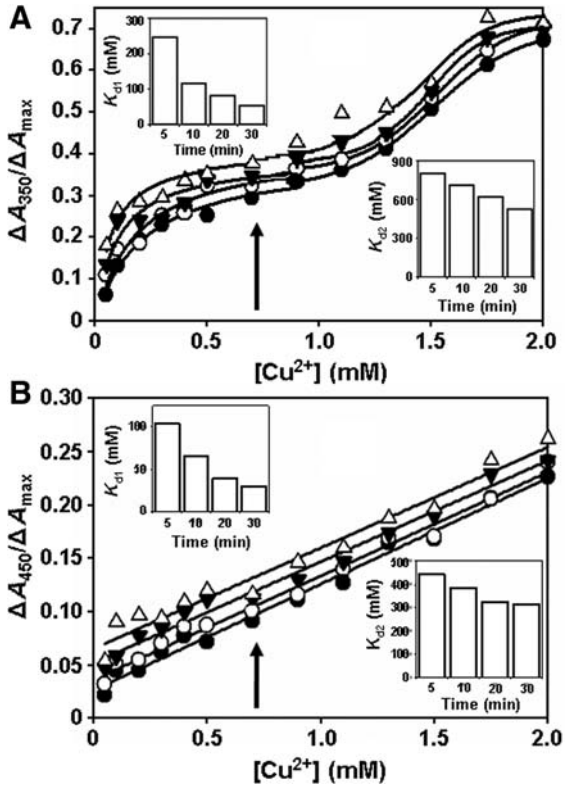


**Figure 5 Plots of the ratio of $\Delta A_{350}/\Delta A_{max}$ vs. $[Cu^{2+}]$ (A), and $\Delta A_{450}/\Delta A_{max}$ vs. $[Cu^{2+}]$ (B)** $\Delta A_{350}$ (or $\Delta A_{450}$) is the absorbance change caused by a given $Cu^{2+}$ concentration at the specified wavelength and $\Delta A_{max}$ is the absorbance change for complete formation of the XO/$Cu^{2+}$ complex as seen at that wavelength. For (A) and (B), data were obtained after XO and $Cu^{2+}$ were pre-incubated for 5 min (filled circle), 10 min (open circle), 20 min (▾), and 30 min (triangle). Insets: value of the apparent dissociation constants $K_{d1}$ and $K_{d2}$ as a function of the pre-incubation time. Arrows indicate the transition between the two $Cu^{2+}$ concentration ranges, below (0.05–0.7 mM) and above (0.7–2 mM) the critical concentration of 0.7 mM.

Values for the Gibbs free energy of binding, calculated according to Equation (2) for each reactive center, are listed in **Table 2**. The observed decrease in values with time illustrated a progressive stabilization of the metal–enzyme complex. The higher values found for $\Delta G_{binding2}$ indicated that the sites filled at higher $Cu^{2+}$ concentrations were characterized by a lower affinity for the metal.

$$\Delta G_{binding} = RT\ln(K_d) \qquad (2)$$

*Characterization of the binding of $Cu^{2+}$ by XO* **Figures 5** and **6** show plots of $\Delta A/\Delta A_{max}$ vs. $[Cu^{2+}]$ obtained for each reactive center after various incubation times of XO with $Cu^{2+}$. $\Delta A_{max}$ was evaluated from the intercept of

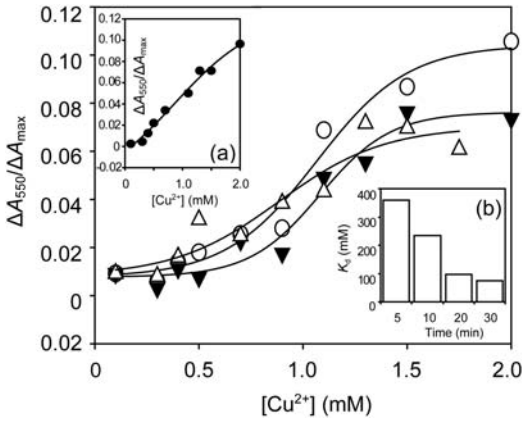


**Figure 6 Plot of the ratio of $\Delta A_{550}/\Delta A_{max}$ vs. $[Cu^{2+}]$** The plot of ratio of $\Delta A_{550}/\Delta A_{max}$ vs. $[Cu^{2+}]$, where $\Delta A_{550}$ is the absorbance change caused by a given $Cu^{2+}$ concentration and $\Delta A_{max}$ is the absorbance change for complete formation of the XO/$Cu^{2+}$ complex as seen at 550 nm. Data were obtained after XO and $Cu^{2+}$ were pre-incubated for 5 min (filled circle) (inset a), 10 min (open circle), 20 min (▾), and 30 min (triangle). Inset b: value of the apparent dissociation constant $K_d$ as a function of the pre-incubation time.

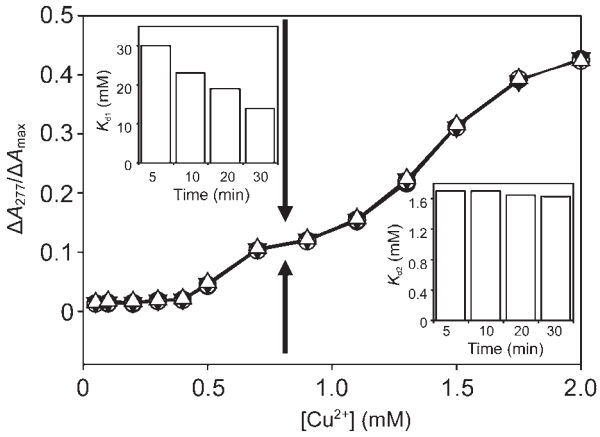


**Figure 7 Plot of the ratio of $\Delta A_{277}/\Delta A_{max}$ vs. $[Cu^{2+}]$** $\Delta A_{277}$ is the absorbance change caused by a given $Cu^{2+}$ concentration and $\Delta A_{max}$ is the absorbance change for complete formation of the XO/$Cu^{2+}$ complex as seen at 277 nm. Data were obtained after XO and $Cu^{2+}$ were pre-incubated for 5 min (filled circle), 10 min (open circle), 20 min (▾), and 30 min (triangle). Insets: value of the apparent dissociation constants $K_{d1}$ and $K_{d2}$ as a function of the pre-incubation time. Arrows indicate the transition between the two $Cu^{2+}$ concentration ranges, below (0.05–0.7 mM) and above (0.7–2 mM) the critical concentration of 0.7 mM.

the plot of $1/\Delta A$ vs. $1/[Cu^{2+}]$ by extrapolation for low-ligand concentration.

The plots shown in **Fig. 5(A)** were obtained for the changes in absorption at 350 nm. Each plot corresponded to a given pre-incubation period (5, 10, 20, and 30 min) and could be decomposed into two parts [separated by the arrow in **Fig. 5(A)**]. The first part, hyperbolic, corresponded to $Cu^{2+}$ concentrations ranging from 0.05 to 0.7 mM and the second, sigmoid, corresponded to $Cu^{2+}$ concentrations ranging from 0.7 to 2 mM. The hyperbolic plots were fits of the data to Equation (3) which is typical for one site saturation ligand binding, whereas the sigmoid plots suggested cooperative ligand binding.

$$y = Ax/B + x \tag{3}$$

These results, along with the values of $K_{d1}$ and $K_{d2}$ obtained from the absorbance changes at 350 nm, suggested that, in the vicinity of the molybdenum center, a first metal-binding site was promptly filled at low $Cu^{2+}$ concentrations while filling of additional metal-binding sites, exhibiting lower affinity for $Cu^{2+}$, did not start before $Cu^{2+}$ concentration reached 0.7 mM. The Hill coefficient, $h$, calculated from the plot of log $[\Delta A_{350}/(\Delta A_{max} - \Delta A_{350})]$ vs. log $[Cu^{2+}]$ was equal to $1.1 \pm 0.1$ for $Cu^{2+}$ concentrations ranging from 0.05 to 0.7 mM; the value decreased progressively to $0.7 \pm 0.05$ as the pre-incubation time increased to 30 min. It was $2.2 \pm 0.1$ for $Cu^{2+}$ concentrations ranging from 0.7 to 2 mM. These values confirmed that the binding observed for lower $Cu^{2+}$ concentrations was non-cooperative and that the binding observed at higher $Cu^{2+}$ concentrations was cooperative. They also suggested the binding of at least three $Cu^{2+}$ (one at higher affinity site, at least two at lower affinity sites) that would influence the absorbance attributable to the molybdenum center.

The plots shown in **Fig. 5(B)** were obtained for the changes in absorption at 450 nm after various pre-incubation times. All plots were linear for the full range of $Cu^{2+}$ concentrations investigated (0.05–2 mM). These observations, along with the two $K_d$ values obtained from the absorbance changes at 450 nm, suggested the existence of two binding sites with different affinities for $Cu^{2+}$ in the vicinity of the FAD center; however, prompt filling of the first site was not observed here and there was no evidence for cooperative binding. The Hill coefficient, $h$, calculated from the plot of log $[\Delta A_{450}/(\Delta A_{max} - \Delta A_{450})]$ vs. log $[Cu^{2+}]$ was equal to $1.05 \pm 0.1$, regardless of $Cu^{2+}$ concentration or pre-incubation time. This also indicated that the binding of possibly two $Cu^{2+}$ around the FAD center was non-cooperative.

Plots obtained for the changes in absorption at 550 nm are shown in **Fig. 6**. A single sigmoid curve, indicating cooperative binding, was obtained for each pre-incubation time, over the full range of $Cu^{2+}$

**Table 2 Values for XO–$Cu^{2+}$ complex dissociation constants and free energy of binding obtained for the various enzyme's reacting centers after increasing pre-incubation time**

| Absorbance peak (nm) | Pre-incubation time (min) | $K_{d1}$ (mM) | $\Delta G_{binding1}$ (cal $mol^{-1}$) | $K_{d2}$ (mM) | $\Delta G_{binding2}$ (cal $mol^{-1}$) |
|---|---|---|---|---|---|
| 277 | 5 | $30 \pm 3.0$ | $-(2078 \pm 50)$ | $1.70 \pm 0.1$ | $-(3778 \pm 45)$ |
| | 10 | $23 \pm 2.0$ | $-(2235 \pm 50)$ | $1.70 \pm 0.1$ | $-(3778 \pm 45)$ |
| | 20 | $19 \pm 1.0$ | $-(2354 \pm 45)$ | $1.65 \pm 0.1$ | $-(3796 \pm 35)$ |
| | 30 | $14 \pm 1.5$ | $-(2529 \pm 60)$ | $1.63 \pm 0.1$ | $-(3803 \pm 35)$ |
| 350 | 5 | $247 \pm 25$ | $-(829 \pm 58)$ | $807 \pm 90$ | $-(127 \pm 40)$ |
| | 10 | $115 \pm 12$ | $-(1281 \pm 58)$ | $714 \pm 75$ | $-(200 \pm 60)$ |
| | 20 | $81 \pm 8$ | $-(1489 \pm 56)$ | $623 \pm 60$ | $-(280 \pm 50)$ |
| | 30 | $53 \pm 5$ | $-(1740 \pm 53)$ | $530 \pm 38$ | $-(376 \pm 40)$ |
| 450 | 5 | $104 \pm 15$ | $-(1341 \pm 80)$ | $442 \pm 50$ | $-(484 \pm 60)$ |
| | 10 | $65 \pm 9$ | $-(1619 \pm 76)$ | $387 \pm 40$ | $-(562 \pm 60)$ |
| | 20 | $40 \pm 6$ | $-(1907 \pm 83)$ | $324 \pm 35$ | $-(668 \pm 60)$ |
| | 30 | $30 \pm 5$ | $-(2078 \pm 92)$ | $315 \pm 30$ | $-(684 \pm 55)$ |
| 550[a] | 5 | $359 \pm 10$ | $-(607 \pm 20)$ | — | — |
| | 10 | $234 \pm 30$ | $-(861 \pm 70)$ | — | — |
| | 20 | $92 \pm 20$ | $-(1388 \pm 80)$ | — | — |
| | 30 | $74 \pm 10$ | $-(1543 \pm 80)$ | — | — |

[a]Only a single value for $K_d$ was found for this absorbance peak.

concentrations investigated (0.05–2 mM). However, absorbance changes were not detectable until $Cu^{2+}$ concentration reached 0.4 mM (0.3 mM for 30-min pre-incubation). The Hill coefficient, $h$, calculated from the plot of log $[\Delta A_{550}/(\Delta A_{max} - \Delta A_{550})]$ vs. log $[Cu^{2+}]$ was equal to $2.5 \pm 0.1$ after 5-min pre-incubation and to $1.6 \pm 0.1$ after 30-min pre-incubation. This confirmed that the binding around the Fe/S centers was cooperative and it suggested that two or three $Cu^{2+}$ would bind.

As shown in **Figs. 5** and **6**, the absorbance changes detectable at the lowest $Cu^{2+}$ concentrations (0.05–0.3 mM) were those observed at 350 nm. Over the same range of metal concentrations, the absorbance changes observed at 450 nm were more gradual and no change was detectable at 550 nm for $Cu^{2+}$ concentrations $<0.4$ mM, except after 30-min pre-incubation when absorbance changes at 550 nm became detectable starting at 0.3 mM $Cu^{2+}$. The position of the arrows in **Fig. 5** corresponded to 0.7 mM $Cu^{2+}$, the critical concentration beyond which drastic inhibition of the enzymatic activity as well as change in the apparent dissociation constant of the metal–enzyme complex were observed.

*Effect of $Cu^{2+}$ on XO tertiary structure* The absorbance and fluorescence of aromatic amino acids depend predominantly on the nature of the molecular neighborhood of these chromophores. Both properties provide for tools extensively used to probe changes in the tertiary structure of proteins [28–33]. In the present study, profiles of tertiary conformational changes were obtained from changes in the absorption at 277 nm. The plots of $\Delta A_{277}/\Delta A_{max}$ vs. $[Cu^{2+}]$ shown in **Fig. 7**, corresponded each to a given pre-incubation period from 5 to 30 min. All plots were quite similar and could be decomposed into two parts (separated by the arrows in **Fig. 7**), the first corresponding to $Cu^{2+}$ concentrations ranging from 0.05 to 0.7 mM with little absorption change $< 0.5$ mM $Cu^{2+}$ and the second, sigmoid, corresponding to $0.7 \text{ mM} \leq [Cu^{2+}] \leq 2$ mM. Two $K_d$ values were obtained for the absorbance changes at 277 nm, $K_{d1}$ corresponding to lower $Cu^{2+}$ concentrations (0.05–0.7 mM) and $K_{d2}$ corresponding to higher $Cu^{2+}$ concentrations (0.7–2 mM), with $K_{d1}$ being larger than $K_{d2}$. The $h$ coefficient, calculated from the plot of log $[\Delta A_{270}/(\Delta A_{max} - \Delta A_{277})]$ vs. log $[Cu^{2+}]$, was equal to $1.14 \pm 0.1$ after 5-min pre-incubation and to $0.8 \pm 0.05$ after 30-min pre-incubation for the lower $Cu^{2+}$ concentrations range, and it was equal to $3.25 \pm 0.15$ for $Cu^{2+}$ concentrations ranging from 0.7 to 2 mM, regardless of the pre-incubation time. It should be noted that the changes in absorbance observed at 277 nm reflect overall structural alterations in the protein imparted by the binding of $Cu^{2+}$ to various

non-identical sites, whereas the changes in absorbance at 350, 450, or 550 nm reflected local alterations around each reactive centers. The values found for the Hill coefficient pertaining to the absorbance changes at 277 nm indicated a number of independent sites at lower $Cu^{2+}$ concentrations (0.05–0.7 mM) and a number of additional binding sites that were not independent of one another at higher $Cu^{2+}$ concentrations (0.7–2 mM). This was in agreement with the findings of non-cooperative binding at lower $Cu^{2+}$ concentrations and cooperative binding at higher $Cu^{2+}$ concentrations, reported for each reactive center.

The values obtained for $K_{d1}$ from the changes in absorbance at 277 nm characterized the binding of $Cu^{2+}$ to a number of non-equivalent, independent sites and were expectedly smaller than those obtained for any of the individual sites (**Table 2**). The values obtained for $K_{d2}$ characterized $Cu^{2+}$ binding to an even larger number of sites and were smaller than the $K_{d1}$ values, reflecting a stabilization of the metal–enzyme complex, even though the $K_{d2}$ values obtained for $Cu^{2+}$ binding to either the molybdenum center (350 nm) or the FAD center (450 nm) were larger than their corresponding $K_{d1}$ values. As the number of $Cu^{2+}$ per enzyme molecule increases, the value of $K_d$ is expected to decrease even if locally some of the additional binding sites exhibited a lower affinity for the metal than the first binding sites (**Table 2**).

*Effect of $Cu^{2+}$ on XO tertiary structure as studied by fluorescence spectroscopy* The amino acid sequence of each subunit in bovine milk XO includes 10 tryptophan and 34 tyrosine residues [13]. Upon excitation at 295 nm, a single emission peak at 405 nm, attributed to the tryptophan residues, was recorded; it was quenched upon addition of $Cu^{2+}$ [**Fig. 8(A),** inset]. The Stern–Volmer plot shown in **Fig. 8(A)** was linear for $Cu^{2+}$ concentrations up to 0.7 mM and exhibited upward curvature at higher $Cu^{2+}$ concentrations, indicative of static quenching [34]. The Stern–Volmer constant $K_{SV}$, calculated from the plot according to Equation (4), was found equal to 960 $M^{-1}$.

$$F_0/F = 1 + K_{SV}[Q] \quad (4)$$

where $F_0$ is the integrated area of the fluorescence spectrum of the sample before quenching, $F$ is the integrated area of the fluorescence spectrum of the sample after quenching, and [Q] is the concentration of quencher.

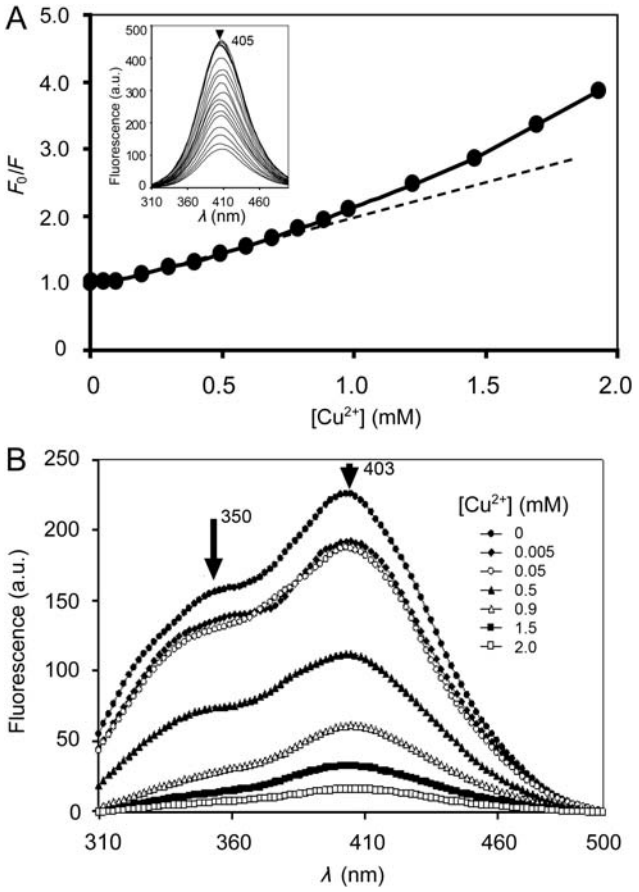


**Figure 8 Stern–Volmer plot and fluorescence emission spectra** (A) Stern–Volmer plot describing tryptophan quenching of XO by $Cu^{2+}$; the plot exhibits upward curvature at higher $Cu^{2+}$ concentrations. The excitation wavelength was 295 nm and the emission spectra of XO and XO in the presence of different [$Cu^{2+}$] (0.005–2 mM) were recorded between 310 and 500 nm; a single peak at 405 nm, attributable to the Tryp residues in the protein, was detectable (inset). (B) Fluorescence emission spectra of XO and XO pre-incubated for 10 min with various $Cu^{2+}$ concentrations from 0.005 to 2 mM, obtained upon excitation at 280 nm. A peak at 405 nm attributable to the Tryp residues and a shoulder at 350 nm attributable to the Tyr residues were detectable. Both peaks decreased with increasing $Cu^{2+}$ concentration.

The fraction of total tryptophan residues accessible for quenching was calculated according to Equation (5), using the modified Stern–Volmer plot.

$$F_0/\Delta F = 1/K_{SV}f_a 1/[Q] + 1/f_a \quad (5)$$

where $\Delta F$ is equal to $F_0 - F$ and $f_a$ is the fraction of accessible fluorophores; $F_0$, $F$, and [Q] are as defined above. The ordinate intercept of the plot of $F_0/\Delta F$ vs. 1/[Q] provides the accessible fluorophores at infinite

quencher concentration and the value found in this case was 30%, thus three tryptophans.

Upon excitation at 280 nm, the emission spectrum of XO exhibited a shoulder at 350 nm in addition to the peak at 405 nm previously observed; both emissions were quenched upon addition of $Cu^{2+}$ [**Fig. 8(B)**]. As evidenced by the normalized spectra shown in **Fig. 9**, for $Cu^{2+}$ concentrations $< 0.7$ mM (0.005–0.5 mM) quenching was more drastic for the emission at 405 nm than for that at 350 nm and was accompanied by a 5-nm blue-shift of both peaks. For $Cu^{2+}$ concentrations that were above 0.7 mM (0.9–2 mM), the emission at 350 nm was quenched as well, and the emission maxima returned at 405 and 350 nm (**Fig. 9**). The differential quenching was also documented by changes in the fluorescence intensity ratio $I_{405}/I_{350}$ (**Fig. 9**, inset).

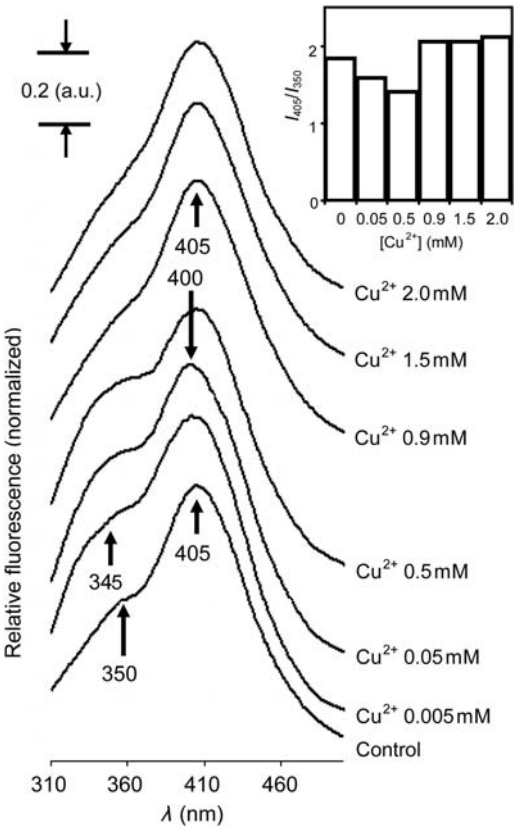


**Figure 9 Normalized fluorescence emission spectra of XO and XO pre-incubated for 10 min with various $Cu^{2+}$ concentrations** The $Cu^{2+}$ concentration is from 0.005 to 2 mM, and the spectra were obtained upon excitation at 280 nm. At low $Cu^{2+}$ concentrations (0.005–0.5 mM) quenching was more drastic for the emission at 405 nm than for that at 350 nm and was accompanied by a 5-nm blue-shift of both peaks; at higher $Cu^{2+}$ concentrations (0.9–2 mM) quenching of the emission at 350 nm occurred and, simultaneously both peaks shifted back to their original position, respectively, at 350 and 405 nm. Inset: ratio $I_{405}/I_{350}$ at different $Cu^{2+}$ concentrations, where $I$ is the fluorescence intensity.

*Effect of $Cu^{2+}$ on XO secondary structure* Far-UV CD spectra taken immediately after addition of increasing concentrations of $Cu^{2+}$ to XO and after 30-min pre-incubation of the enzyme with the metal, are shown in **Fig. 10(A** and **B),** respectively. Secondary structure fractions were calculated using the CD spectra deconvolution program CDNN version 2.1 (http://bioinformatik.biochemtech.uni-halle.de/cdnn); changes in the fraction of various secondary structure elements as a function of $Cu^{2+}$ concentration and pre-incubation time are shown in **Fig. 10(C–F).** The changes were metal concentration- as well as time-dependent and affected essentially the $\alpha$-helical content and $\beta$-sheet fraction of the enzyme. Upon addition of $Cu^{2+}$, the $\alpha$-helical content increased by up to 12% for metal concentrations up to 1 μM, and then began to decrease, reaching 62% of the control in 2 mM $Cu^{2+}$. After 5-min pre-incubation of the enzyme with the metal, increases in the $\alpha$-helical content were no longer observed; instead decreases going from 8% for 1 μM $Cu^{2+}$ to 44% for 2 mM $Cu^{2+}$ were recorded. With prolonged pre-incubation, the $\alpha$-helical content further diminished with a 16% reduction for 1 μM $Cu^{2+}$ and up to a 56% reduction for 2 mM $Cu^{2+}$ [**Fig. 10(C)**]. Concomitantly, increases in the $\beta$-sheet fraction were recorded that went from a 9% increase with 1 μM $Cu^{2+}$ to a 37% increase with 2 mM $Cu^{2+}$ immediately after addition of the metal. As the pre-incubation time between XO and $Cu^{2+}$ increased, so did the $\beta$-sheet fraction; after 30-min pre-incubation, there was a 30% increase in $\beta$-sheet with $Cu^{2+}$ 1 μM and a 49% increase with 2 mM $Cu^{2+}$ [**Fig. 10(D)**]. Only moderate changes were observed in the $\beta$-turn content with a maximum increase of 20% observed after 30-min pre-incubation with 2 mM $Cu^{2+}$ [**Fig. 10(E)**]. The random coil fraction remained essentially unchanged except that it increased by 5–8% with 2 mM $Cu^{2+}$ as the pre-incubation time increased to 30 min [**Fig. 10(F)**].

*Effect of $Cu^{2+}$ on the visible portion of XO CD spectrum* CD spectra of XO and XO in the presence of various $Cu^{2+}$ concentrations were also recorded in the visible region, from 350 to 700 nm (**Fig. 11**). The native enzyme exhibited a peak at 432 nm, one at 450 nm and a trough at 550 nm. Addition of 0.1 mM $Cu^{2+}$ caused a decrease in the peaks at 432 and 450 nm and a deepening of the trough at 550 nm, but the proportion between

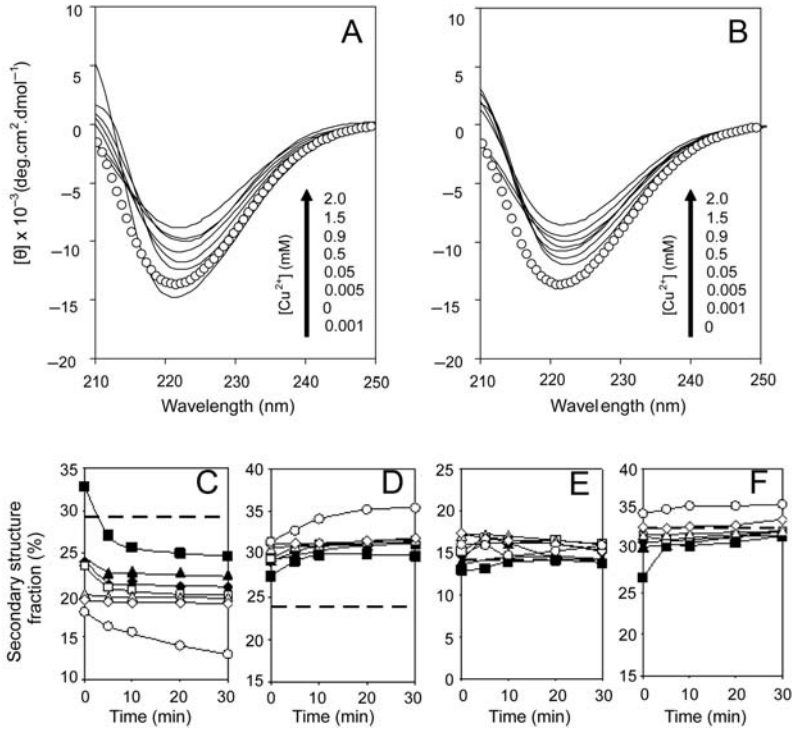


**Figure 10 Far-UV CD spectra analysis** Far-UV CD spectra taken (A) immediately after addition of increasing concentrations of $Cu^{2+}$ to XO and (B) after 30-min pre-incubation of the metal with the enzyme. Changes in the $\alpha$-helical fraction (C), the $\beta$-sheet fraction (D), the $\beta$-turn fraction (E), and the random coil fraction (F) of the enzyme pre-incubated with various $Cu^{2+}$ concentrations as a function of the time of pre-incubation. (filled square) 0.001 mM $Cu^{2+}$, (filled triangle) 0.005 mM $Cu^{2+}$, (filled diamond) 0.05 mM $Cu^{2+}$, (open square) 0.5 mM $Cu^{2+}$, (triangle) 0.9 mM $Cu^{2+}$, (diamond) 1.5 mM $Cu^{2+}$, (open circle) 2 mM $Cu^{2+}$. The dotted lines represent the control value for the enzyme in the absence of $Cu^{2+}$.

the 432- and 450-nm peaks remained unchanged. Similar observations were made whether the enzyme and the metal were pre-incubated for 0 min [**Fig. 11(A)**] or 30 min [**Fig. 11(B)**] except for a slight enhancement of the effect after 30 min. Addition of 0.5 mM $Cu^{2+}$ led to a CD spectrum similar to the control, except for a deeper trough at 550 nm [**Fig. 11(A)**]; after 30-min pre-incubation, the same peaks were obtained in the same proportions but they were ~20% smaller [**Fig. 11(B)**]. When XO was exposed to 1.5 mM $Cu^{2+}$, a metal concentration causing drastic inhibition of the enzymatic activity, the visible CD spectrum exhibited an enhanced signal at 432 nm (17% increase) and, especially, at 450 nm (28% increase); this resulted in an inverse proportion of the 432-nm peak vs. the 450-nm peak compared with the control [**Fig. 11(A)**]. After 30-min pre-incubation, the signals decreased so that the 450-nm peak was similar in height to the control while that at 432 nm was 12% lower than the control, changing the ratio 432/450 nm from 1.06 for the control to 0.94 in the presence of $Cu^{2+}$ [**Fig. 11(B)**].

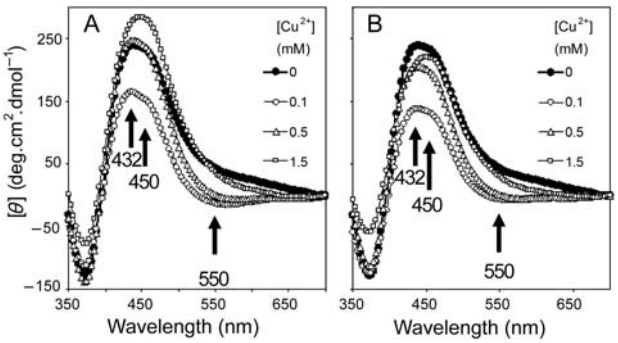


**Figure 11 Visible region CD spectra of XO taken (A) immediately after addition of increasing concentrations of $Cu^{2+}$ to the enzyme and (B) after 30-min pre-incubation of the metal with the enzyme.**

## Discussion

The enzymatic activity studies presented here showed that $Cu^{2+}$ was a reversible inhibitor as well as an activator of the XO-catalyzed oxidation of xanthine to uric acid. The spectroscopic studies showed that $Cu^{2+}$ formed

a complex with XO that resulted in specific alterations around each reactive center along with alterations in the secondary and, eventually, tertiary structure of the enzyme. Binding studies based on absorbance changes at 350, 450, and 550 nm showed that the alterations detectable at the lowest $Cu^{2+}$ concentrations (starting at 0.05 mM) took place around the molybdenum center with prompt saturation of a binding site. Over the same metal concentration range, alterations were also detectable around the FAD center but to a lesser extent and with no binding site saturation. Alterations around the Fe/S centers, as revealed by absorbance decreases at 550 nm were not detectable until $Cu^{2+}$ concentration reached 0.4 mM. Absorbance changes at 277 nm were mostly negligible until 0.5 mM $Cu^{2+}$, indicating that the initial alterations around the molybdenum and FAD centers affected essentially the secondary structure of the enzyme. The far-UV CD data revealed that indeed alterations in the secondary structure of the enzyme were detectable at the lowest $Cu^{2+}$ concentrations probed.

Exposure of XO to $Cu^{2+}$ concentrations above a critical value of 0.7 mM, led to drastic inhibition of the enzymatic activity that coincided with the cooperative binding of additional $Cu^{2+}$ around the molybdenum center, the binding of an additional $Cu^{2+}$ around the FAD center and the progressive binding of probably three $Cu^{2+}$ around the Fe/S centers. Drastic absorbance changes were observed at 277 nm, indicating alterations to the tertiary structure while far-UV CD data reflected further alterations in the secondary structure.

The change in inhibition type from non-competitive to mixed observed with prolonged pre-incubation (over 10 min) of XO with $Cu^{2+}$ coincided with progressive saturation of the sites occupied by the metal, especially around the Fe/S centers, and with increased stability of the XO–Cu complex as indicated by the decreasing $K_d$ and $\Delta G$ values.

Determination of the apparent dissociation constant of the metal–enzyme complex, based on the absorbance changes observed for the molybdenum center and for the FAD center, revealed two constants ($K_{d1}$ and $K_{d2}$) in each case, indicating the existence of sites with lower affinity for $Cu^{2+}$ that would be filled only after the metal concentration reached the critical value of 0.7 mM. In parallel with the kinetics results, filling of lower affinity sites led to complete inactivation of the enzyme, while filling of higher affinity sites resulted in limited inhibition of the enzymatic activity. Cooperative binding along with a single $K_d$ value were deduced from the absorbance changes observed for the Fe/S centers.

Consensus sequences for $Cu^{2+}$ binding sites have been established, with His or Cys often identified as the anchoring amino acid [35–37]. To determine the precise location of the $Cu^{2+}$ binding sites in XO would require X-ray crystallography of the metal–enzyme complex. However, the information gathered by various groups on the enzyme structure [8,13,14] allowed us to make some predictions regarding plausible binding sites for $Cu^{2+}$. A close examination of the enzyme structure reveals that XO exhibits a number of potential binding sites for $Cu^{2+}$ in the vicinity of each of its reactive centers. **Figure 12** provides a schematic representation of the reactive centers with some His and Cys residues located near them along with the amino acids reported to be involved in the substrate binding and the reaction catalysis [8,13–15]. Most of these residues are deeply buried in the protein but some, like $His^{875}$, $His^{67}$, and $His^{82}$ (underlined in **Fig. 12**), are more exposed and thus more accessible to $Cu^{2+}$. $His^{875}$, in the molybdopterin-binding domain, is part of a sequence that includes $Arg^{880}$, one of the key amino acids maintaining the substrate in the proper orientation [38]. It is likely to be part of the first binding site, leading to alterations in the molybdenum

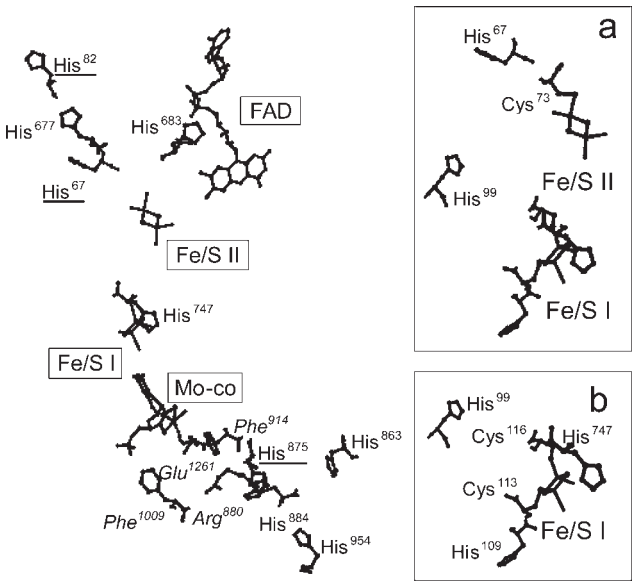


**Figure 12 Relative orientations of the reactive centers in bovine milk XO and His residues potentially involved in $Cu^{2+}$ binding** Residues important in substrate binding and reaction catalysis are also indicated and labeled in italics characters. The labels for the most exposed His residues are underlined. Insets: additional His and Cys residues potentially involved in $Cu^{2+}$ binding around the Fe/S II (a) and Fe/S I (b) centers. Images generated using the Swiss-PdbViewer (http://www.expasy.ch/spdbv) from the data of Enroth *et al*. [13].

center environment and hampering substrate binding (**Fig. 12**). However, as indicated by the pH profiles obtained in the presence of various $Cu^{2+}$ concentrations, the binding did not affect ionization of $Glu^{1261}$ that is involved in the reaction catalysis [16]. Next, the FAD center was altered and the sequence including $His^{82}$ is a likely binding site. $His^{82}$, in the iron–sulfur-binding domain, is part of the sequence $Ile^{77}Cys^{78}Thr^{79}Leu^{80}His^{81}His^{82}Val^{83}Ala^{84}Val^{85}Thr^{86}$ that is near the FAD center; the sequence also includes $His^{81}$ and $Cys^{78}$ residues. Subsequent alterations around the Fe/S centers were possibly initiated with binding at the sequence including $His^{67}$ at low $Cu^{2+}$ concentrations, leading to increasing alterations of the electron transfer to $O_2$ and increasing inhibition of enzymatic activity. $His^{67}$ is part of the sequence $Lys^{64}Ile^{65}Ile^{66}His^{67}Phe^{68}Ser^{69}Ala^{70}Asn^{71}Ala^{72}$ $Cys^{73}Leu^{74}Ala^{75}Pro^{76}$ that is close to the FAD center and also includes $Cys^{73}$ residue to which Fe/S II is coordinated. In the vicinity of the Fe/S I center, the sequence $Lys^{95}Thr^{96}Arg^{97}Leu^{98}His^{99}Pro^{100}Val^{101}Gln^{102}Glu^{103}Arg^{104}Ile^{105}Ala^{106}Lys^{107}$ $Ser^{108}$ $His^{109}Gly^{110}Ser^{111}Gln^{112}Cys^{113}$ $Gly^{114}Phe^{115}Cys^{116}Thr^{117}Pro^{118}Gly^{119}$ comprises two His and two Cys residues, providing binding sites for $Cu^{2+}$. At higher $Cu^{2+}$ concentrations corresponding to drastic inhibition of the enzymatic activity, cooperative binding around the Fe/S centers continued, involving less accessible His and Cys residues. $His^{677}$ and $His^{683}$ are deeply buried residues, part of the molybdopterin-binding domain but close to the FAD center; prior binding of $Cu^{2+}$ to the more accessible nearby $His^{67}$ is likely to facilitate binding to residues $His^{677}$ and $His^{683}$. Binding involving residue $His^{683}$ is likely to affect the Fe/S II center as well as the FAD center (**Fig. 12**). The cooperative binding observed around the molybdenum center at higher $Cu^{2+}$ concentrations could involve residues $His^{863}$ and $His^{954}$; alternatively, residue $His^{109}$ in the vicinity of the Fe/S I center could also affect the molybdenum center. Thus, from three potential binding sites around the molybdenum center, one was probably common to the molybdenum and the Fe/S I centers; and from two potential binding sites around the FAD center, one was probably common to the FAD and the Fe/S II centers.

In limited concentrations and after brief pre-incubation with XO, $Cu^{2+}$ would enhance rather than inhibit the enzymatic activity. A similar phenomenon was seen in the study of the effect of $Ni^{2+}$ on horseradish peroxidase activity [39]. As previously suggested, this transient activity stimulation could be due to a stabilization of the enzyme in its optimal conformation. Approximately one-third of all proteins are completely or partially unfolded [40] and metals bind with higher affinity to the folded state than to the unfolded state or partially folded states of a protein [41]. It is likely that when $Cu^{2+}$ was in low concentration, binding first occurred with the completely folded enzyme. With extended pre-incubation time, or higher $Cu^{2+}$ concentrations, binding to the other states of the enzyme took place and, eventually multiple binding sites were filled leading to increasing inhibition of the activity.

*Conflict of interest statement*. None declared.

## Funding

This work was supported in part by the J. and E. Research Foundation, Tehran, Iran.

## References

1 Uauy R, Olivares M and Gonzalez M. Essentiality of copper in humans. Am J Clin Nutr 1998, 67: 952S–959S.
2 Balamurugan K and Schaffner W. Copper homeostasis in eukaryotes: teetering on a tightrope. Biochim Biophys Acta 2006, 1763: 737–746.
3 Keyhani E and Keyhani J. Identification of porphyrin present in apo-cytochrome c oxidase of copper-deficient yeast cells. Biochim Biophys Acta 1980, 633: 211–227.
4 Percival SS and Harris ED. Regulation of Cu, Zn superoxide dismutase with copper. Caeruloplasmin maintains levels of functional enzyme activity during differentiation of K562 cells. Biochem J 1991, 274: 153–158.
5 Llamas A, Otte T, Multhaup G, Mendel RR and Schwarz G. The mechanism of nucleotide- assisted molybdenum insertion into molybdopterin. A novel route toward metal cofactor assembly. J Biol Chem 2006, 281: 18343–18350.
6 Brewer GJ and Yuzbasiyan-Gurkan V. Wilson disease. Medicine 1992, 71: 139–164.
7 Keyhani E, Abdi-Oskouei F, Attar F and Keyhani J. DNA strand breaks by metal-induced oxygen radicals in purified *Salmonella typhimurium* DNA. Ann NY Acad Sci 2006, 1091: 52–64.
8 Harrison R. Structure and function of xanthine oxidoreductase: Where are we now. Free Rad Biol Med 2002, 33: 774–797.
9 Parks DA and Granger DN. Xanthine oxidase: biochemistry, distribution and physiology. Acta Physiol Scand 1986, 548: 87–99.
10 Doehner W and Anker SD. Xanthine oxidase inhibition for chronic heart failure: is allopurinol the next therapeutic advance in heart failure. Heart 2005, 91: 707–709.
11 Berry CE and Hare JM. Xanthine oxidoreductase and cardiovascular disease: molecular mechanisms and pathophysiological implications. J Physiol 2004, 555: 589–606.
12 McCord JM. Oxygen-derived free radicals in postischemic tissue injury. N Engl J Med 1985, 312: 159–163.
13 Enroth C, Eger BT, Okamoto K, Nishino T and Pai E. Crystal structures of bovine milk xanthine dehydrogenase and xanthine oxidase:

structure based mechanism of conversion. Proc Natl Acad Sci USA 2000, 97: 10723–10728.
14 Hille R. The mononuclear molybdenum enzymes. Chem Rev 1996, 96: 2757–2816.
15 Huber R, Hof P, Duarte RO, Moura JG, Moura I, Liu MY and LeGall J, *et al*. A structure-based catalytic mechanism for the xanthine oxidase family of molybdenum enzymes. Proc Natl Acad Sci USA 1996, 93: 8846–8851.
16 Doonan CJ, Stockert A, Hille R and George GN. Nature of the catalytically labile oxygen at the active site of xanthine oxidase. J Am Chem Soc 2005, 127: 4518–4522.
17 Godber BLJ, Schwarz G, Mendel RR, Lowe DJ, Bray RC, Eisenthal R and Harrison R. Molecular characterization of human xanthine oxidoreductase: the enzyme is grossly deficient in molybdenum and substantially deficient in iron–sulphur centers. Biochem J 2005, 388: 501–508.
18 Ventom AM, Deistung J and Bray RC. The isolation of demolybdo xanthine oxidase from bovine milk. Biochem J 1988, 255: 949–956.
19 Bastian NR, Kay CJ, Barber MJ and Rajagopalan KV. Spectroscopic studies of the molybdenum-containing dimethyl sulfoxide reductase from *Rhodobacter sphaeroides f.* sp. *Denitrificans*.. J Biol Chem 1991, 266: 45–51.
20 Lee C, Liu X and Zweier JL. Regulation of xanthine oxidase by nitric oxide and Peroxynitrite. J Biol Chem 2000, 275: 9369–9376.
21 Fernandes AS, Gaspar J, Cabral MF, Caneiras C, Guedes R, Rueff J and Castro M, *et al*. Macrocyclic copper (II) complexes: superoxide scavenging activity, structural studies and cytotoxicity evaluation. J Inorg Biochem 2007, 101: 849–858.
22 Sau AK, Mondal MS and Mitra S. Interaction of $Cu^{2+}$ ion with milk xanthine oxidase. Biochim Biophys Acta 2001, 1544: 89–95.
23 Mondal MS and Mitra S. The inhibition of bovine xanthine oxidase activity by $Hg^{2+}$ and other metal ions. J Inorg Biochem 1996, 62: 271–279.
24 Ghio AJ, Kennedy TP, Stonehuerner J, Carter JD, Skinner KA, Parks DA and Hoidal JR. Iron regulates xanthine oxidase activity in the lung. Am J Physiol Lung Cell Mol Physiol 2002, 283: L563–L572.
25 Løvstad RA. A kinetic study on iron stimulation of the xanthine oxidase dependent oxidation of ascorbate. BioMetals 2003, 16: 435–439.
26 Hadizadeh M, Khodadadi C, Keyhani E and Keyhani J. Kinetics and spectrophotometric studies of the effect of copper on xanthine oxidase. FEBS J 2008, 275: 219.
27 Edmondson D, Massey V, Palmer G, Beacham LM and Elion GB. The resolution of active and inactive xanthine oxidase by affinity chromatography. J Biol Chem 1972, 247: 1597–1604.
28 Schejter A, Lanir A and Epstein N. Binding of hydrogen donors to horseradish peroxidase: a spectroscopic study. Arch Biochem Biophys 1976, 174: 36–44.
29 Keyhani J, Keyhani E, Einollahi N, Minai-Tehrani D and Zarchipour S. Heterogenous inhibition of horseradish peroxidase activity by cadmium. Biochim Biophys Acta 2003, 1621: 140–148.
30 Casella L, Gullotti M, Poli S, Bonfa M, Ferrari RP and Marchesini A. Spectroscopic and binding studies on the stereoselective interaction of tyrosine with horseradish peroxidase and lactoperoxidase. Biochem J 1991, 279: 245–250.
31 Youngs HL, Sundaramoorthy M and Gold MH. Effect of cadmium on manganese peroxidase competitive inhibition of MnII oxidation and thermal stabilization of the enzyme. Eur J Biochem 2000, 267: 1761–1769.
32 Smulevich G, Paoli M, Sanctis GD, Mantini AR, Ascoli F and Coletta M. Spectroscopic evidence for a conformational transition in horseradish peroxidase at very low pH. Biochemistry 1997, 36: 640–649.
33 Choi DW, Zea CJ, Do YS, Senrau JD, Antholine WE, Hargrove MS and Pohl NL, *et al*. Spectral, kinetic and thermodynamic properties of Cu(I) and Cu(II) binding by Methanobactin from *Methylosinus trichosporium* OB3b. Biochemistry 2006, 45: 1442–1453.
34 Soares S, Mateus N and de Freitas V. Interaction of different polyphenols with bovine serum albumin (BSA) and human salivary $\alpha$-amylase (HAS) by fluorescence quenching. J Agric Food Chem 2007, 55: 6727–6735.
35 Burns CS, Aronoff-Spencer E, Legname G, Prusiner SB, Antholine WE, Gerfen GJ and Peisach J, *et al*. Copper-coordination in the full-length, recombinant prion protein. Biochemistry 2003, 42: 6794–6803.
36 Valensin D, Mancini FM, Luckowski M, Janicka AK, Wiśniewska AK, Gaggelli E and Valensin G, *et al*. Identification of a novel high affinity copper binding site in the APP(145–155) fragment of amyloid precursor protein. Dalton Trans 2004, 16–22.
37 Karavelas T, Mylonas M, Malandrinos G, Plakatouras JC, Hadjiliadis N, Mlynarz P and Kozlowski H. Coordination properties of Cu(II) and Ni(II) ions towards the C-terminal peptide fragment—ELAKHA of histone H2B. J Inorg Biochem 2005, 99: 606–615.
38 Pauff JM, Zhang J, Bell CE and Hille R. Substrate orientation in xanthine oxidase: crystal structure of enzyme in reaction with 2-hydroxy-6-methylpurine. J Biol Chem 2008, 283: 4818–4824.
39 Tayefi-Nasrabadi H, Keyhani E and Keyhani J. Conformational changes and activity alterations induced by nickel ion in horseradish peroxidase. Biochimie 2006, 88: 1183–1197.
40 Schreiber G and Serrano L. Folding and binding: an extended family business. Curr Opin Struct Biol 2005, 15: 1–3.
41 Arnold FH and Zhang JH. Metal-mediated protein stabilization. Trends Biotechnol 1994, 12: 189–192.